Transition between Electron Localization and Antilocalization in Graphene

F. V. Tikhonenko, A. A. Kozikov, A. K. Savchenko, and R. V. Gorbachev
School of Physics, University of Exeter, EX4 4QL Exeter, United Kingdom
(Received 16 July 2009; published 23 November 2009)

We show that quantum interference in graphene can result in antilocalization of charge carriers—an increase of the conductance, which is detected by a negative magnetoconductance. We demonstrate that depending on experimental conditions one can observe either weak localization or antilocalization of carriers in graphene. A transition from localization to antilocalization occurs when the carrier density is decreased and the temperature is increased. We show that quantum interference in graphene can survive at high temperatures, up to $T \sim 200$ K, due to weak electron-phonon scattering.

DOI: 10.1103/PhysRevLett.103.226801 PACS numbers: 73.23.−b, 72.15.Rn, 73.43.Qt

Quantum interference in graphene, a monolayer of carbon atoms, is very different from that in conventional two-dimensional (2D) systems due to *chirality* of charge carriers and an additional quantum number, the pseudospin [1,2]. The carriers in graphene have a Berry phase of π: the additional phase that the electron wave function will acquire if an electron completes a closed trajectory. This should result in weak antilocalization (WAL) of charge carriers compared with the conventional localization (WL) in 2D systems [3,4].

Figure 1(a) shows how an electron scattered by impurities can interfere on a closed trajectory when it is treated as a wave. Two electron waves propagate in opposite directions around the trajectory and interfere at the point of intercept. As the two paths are identical, the phase of the two waves is the same and the interference constructive. This increases the probability for electrons to scatter back and decreases the electrical conductance compared with its classical Drude value. In experiment, the quantum correction to the conductance is usually detected by applying a magnetic field perpendicular to the 2D system. It adds a phase difference to the two waves and destroys the interference. This results in an increase of the conductance—positive magnetoconductance (MC), $\Delta\sigma(B) = \sigma(B) - \sigma(B = 0) > 0$. In graphene, however, the Berry phase π adds a phase difference to the two interfering trajectories, so that they meet in antiphase and destructive interference occurs. This should result in an increase of the conductance due to quantum interference and a negative magnetoconductance [1]. This antilocalization effect is very different from that observed before in 2D systems with strong spin-orbit scattering [3,5–8] where the two waves meet in antiphase because of spin flips in scattering by impurities—in graphene spin-orbit interaction is known to be weak due to the low mass of carbon atoms [9].

So far the experimental studies of quantum interference in graphene-based systems have not revealed negative magnetoconductance [10–14], although the observed weak localization has been seen to be unusual in that it depends not only on inelastic scattering of electrons, characterized by the dephasing time τ_ϕ, but also on elastic scattering caused by impurities and imperfections in the crystal structure. Weak antilocalization was expected to be seen only in samples without defects, i.e., in the absence of intervalley scattering and chirality breaking scattering by atomically sharp defects. In this work we present clear evidence for WAL in graphene by observing negative MC at low magnetic fields. We establish the experimental conditions for its observation and show that in mechanically exfoliated graphene one is able to detect negative MC even in the presence of such scattering. We demonstrate that in the same sample a transition between localization and antilocalization can be seen by changing temperature and electron density.

The theory [1] of quantum interference has been shown to be applicable to the description of the MC in mechanically exfoliated graphene [12] and a graphitic system on the surface of SiC [10]:

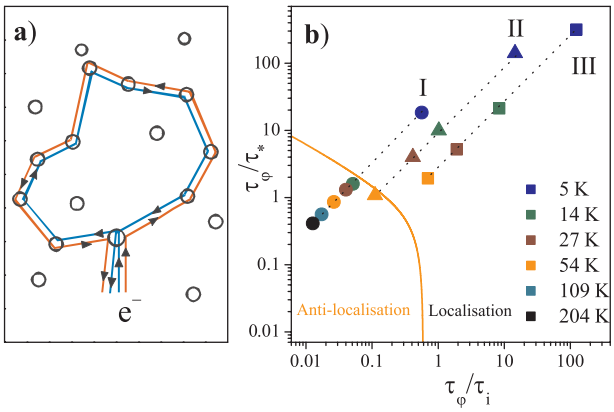

FIG. 1 (color online). (a) The trajectories of an electron scattered by impurities that give rise to a quantum correction to the conductance. (b) A diagram of the scattering times related to quantum interference in graphene. The solid curve separates the regions of electron localization and antilocalization. Points are experimental values found from the analysis of the magnetoconductance using Eq. (1), for three regions of electron density.

$$\Delta\sigma(B) = \frac{e^2}{\pi h}\left(F\left(\frac{\tau_B^{-1}}{\tau_\phi^{-1}}\right) - F\left(\frac{\tau_B^{-1}}{\tau_\phi^{-1} + 2\tau_i^{-1}}\right) - 2F\left(\frac{\tau_B^{-1}}{\tau_\phi^{-1} + \tau_i^{-1} + \tau_*^{-1}}\right)\right). \quad (1)$$

Here $F(z) = \ln z + \psi(0.5 + z^{-1})$, $\psi(x)$ is the digamma function, $\tau_B^{-1} = 4eDB/\hbar$ and D is the diffusion coefficient. (The theory assumes that the momentum relaxation rate τ_p^{-1} is the highest in the system and comes from charged impurities, and does not affect the electron interference.) The quantum correction depends not only on the dephasing time τ_ϕ but on elastic scattering times τ_i and τ_*. Graphene's band structure has two valleys, and quantum interference of electrons in one valley can be suppressed by scattering on the defects with the size of the lattice spacing, as well as dislocations and ripples [1,2,15]. Such defects break the chirality, while dislocations and ripples produce an effective random magnetic field which destroys the interference. The combined effect of this intravalley scattering is characterized by the time τ_*. Intervalley scattering by sharp defects (such as the edges of the sample) that are able to scatter electrons between the two valleys is characterized by the time τ_i. While small τ_* suppresses interference within a valley, small enough τ_i restores it by mixing the two valleys, which have opposite chirality.

Negative MC corresponding to antilocalization is determined by (negative) second and third terms in Eq. (1). In the absence of intra- and intervalley scattering in a defect-free graphene layer, $\tau_{i,*} \to \infty$, $\Delta\sigma(B)$ is totally controlled by the third term. In the opposite case of strong intra- and intervalley scattering (small τ_* and τ_i), both negative terms are suppressed and the first (positive) term dominates, which corresponds to electron localization. It is this situation that was realized in the experiments [12] on mechanically exfoliated graphene, where the negative terms coming from the chirality of electrons were clearly visible but not large enough to change the sign of the MC in low fields.

Careful analysis of Eq. (1) demonstrates, however, that antilocalization can still be detected in such samples. Using the fact that the function $F(z)$ for $z \ll 1$ (at small magnetic fields) can be represented by a simple quadratic dependence $F(z) = z^2/24$, we simplify Eq. (1) for small fields as

$$\Delta\sigma(B) = \frac{e^2}{24\pi h}\left(\frac{4eDB\tau_\phi}{\hbar}\right)^2\left(1 - \frac{1}{(1 + 2\tau_\phi/\tau_i)^2} - \frac{2}{(1 + \tau_\phi/\tau_i + \tau_\phi/\tau_*)^2}\right). \quad (2)$$

The expression in the brackets determines the sign of the MC. Figure 1(b) shows a diagram with a curve $\Delta\sigma = 0$ that separates the regions of positive and negative MC (localization and antilocalization). The favorable conditions for the observation of negative MC are small ratios τ_ϕ/τ_* and τ_ϕ/τ_i. This can be realized by increasing the temperature (which decreases τ_ϕ) and by lowering the carrier density (which increases τ_i [12]).

The studied sample is produced by mechanical exfoliation of graphite and deposited on an oxidized Si wafer [16]. Using electron-beam lithography a six-terminal Hall bar is formed from the flake with a width of 2 μm and a length between the potential probes (Au/Cr) of 22.5 μm. The sample was annealed in vacuum at a temperature of 140 °C for two hours before cooling down in a cryostat. Figure 2(a) shows a schematic of the measurement circuit. The inset shows the quantum Hall effect where plateaux at half-integer filling factors are evidence that the sample is monolayer graphene [17]. The mobility of electrons outside the Dirac (electro-neutrality) region is $\sim$12 000 cm^2 V^{-1} s^{-1}. The resistance R as a function of the gate voltage V_g shows a peak at the Dirac point where the density of charge carriers is zero. The bars indicate three regions of the gate voltage (of size $\Delta V_g = 1$ V) where the MC is measured. To average out the effect of universal conductance fluctuations [18], the resistance at each magnetic field is averaged over each of the regions. These measurements are then repeated at different temperatures in the range $T = 5$–200 K.

Figures 2(b)–2(d) show the evolution of the MC with changing carrier density at three temperatures. One can see

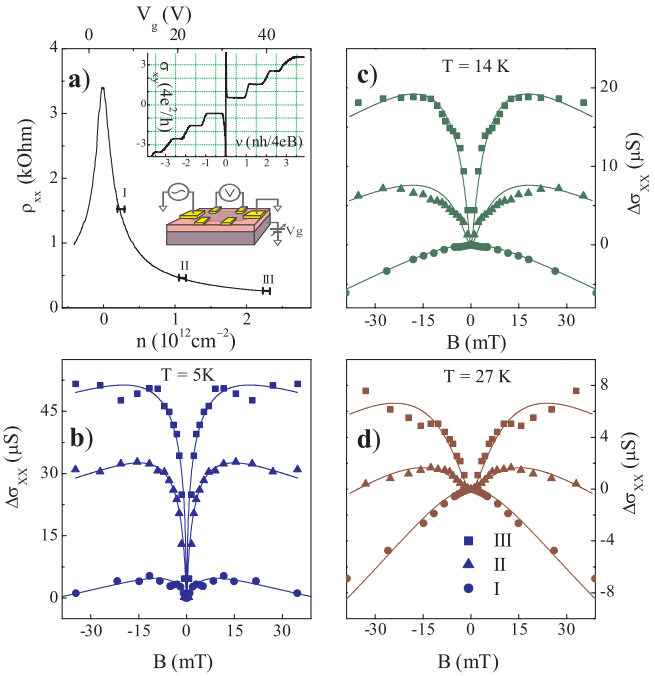

FIG. 2 (color online). (a) Resistivity as a function of the carrier density, with the three regions where the magnetoconductance is studied indicated by bars. Insets: a diagram of the sample and the results of the quantum Hall effect measurement. (b),(c),(d) Evolution of the magnetoconductance with decreasing electron density, at three temperatures. Solid curves are fits to Eq. (1).

that with decreasing density (moving from region III to region I) the MC at $T = 14$ and 27 K changes its sign from positive to negative. Indeed, the ratio of the characteristic times found from the analysis of the MC curves using Eq. (1) is seen to enter the region of antilocalization in Fig. 1(b). (A similar transition between WL and WAL was observed in 2D systems where the strength of spin-orbit scattering was controlled by changing carrier density [7,8].) At $T = 5$ K, however, where the value of τ_ϕ is larger, one cannot achieve the transition to antilocalization, Fig. 1(b).

Figure 3 shows the evolution of the MC with increasing temperature in the three regions of carrier density. It follows from Eq. (1) that at low temperatures the width of the dip in small B is mainly controlled by τ_ϕ, while the bending of the curve at larger B is determined by τ_i and τ_*. The analysis of the MC curves shows that, as expected, elastic times τ_i and τ_* are essentially temperature independent but inelastic time τ_ϕ strongly decreases with increasing T. One can see in Fig. 3 that with increasing T the width of the dip in the MC increases (due to a decrease of τ_ϕ), so that the dependence becomes flat at $T = 27$ K. With further increase of the temperature the quantum correction starts being seen again, but now as a peak in the MC. Its width continues to increase with increasing T, until at $T \sim 200$ K the dependence becomes flat again when antilocalization disappears due to rapid dephasing of the electron trajectories. Note that the transition from WL to WAL is seen in regions I and II, but not in the high-density region III. In this region the intervalley time τ_i becomes too small to satisfy the condition of antilocalization, Fig. 1(b).

Our experiments are performed at much higher temperatures than the previous studies of weak localization in exfoliated graphene [12,13] ($T < 20$ K). In Fig. 3 one can see that the temperature dependent MC exists at temperatures $T \sim 200$ K, while in conventional 2D systems the quantum correction usually disappears at much lower temperatures, due to intensive electron-phonon scattering [19]. In graphene, however, electron-phonon scattering is expected to be weak [20,21], and thus it is interesting to examine what the source of dephasing is at high T.

In earlier studies of electron localization [12] the temperature dependence of the dephasing rate τ_ϕ^{-1} was found to follow the linear temperature dependence caused by electron-electron scattering in the "diffusive" regime [22]:

$$\tau_\phi^{-1} = \alpha \frac{k_B T}{2E_F \tau_p} \ln\left(\frac{2E_F \tau_p}{\hbar}\right), \tag{3}$$

where α is a coefficient of the order of unity. This regime corresponds to the condition $k_B T \tau_p/\hbar < 1$, which means that two interacting electrons experience many collisions with impurities during the interaction time $\hbar/k_B T$. Figure 4 shows the dephasing rate, obtained from the analysis of the MC using Eq. (1), in the three regions of carrier density. The expected transport phonon scattering rate in graphene is given by the following relation [20,21]:

$$\tau_{e\text{-ph}}^{-1} = \frac{1}{\hbar^3} \frac{E_F}{4V_F^2} \frac{D_a^2}{\rho_m V_{\text{ph}}^2} k_B T, \tag{4}$$

where D_a is the deformation potential constant, ρ_m is the density of graphene, V_{ph} is the speed of sound, and V_F is the Fermi velocity. Assuming that this scattering rate is close to the dephasing rate due to electron-phonon scattering, $\tau_\phi \sim \tau_{e\text{-ph}}$ [23], we plot it in Fig. 4 using the parameters $\rho_m = 7.6 \times 10^{-7}$ kg m^{-2}, $V_{\text{ph}} = 2 \times 10^4$ m s^{-1}, $V_F = 10^6$ m s^{-1}, and $D_a \approx 18$ eV taken from the analysis

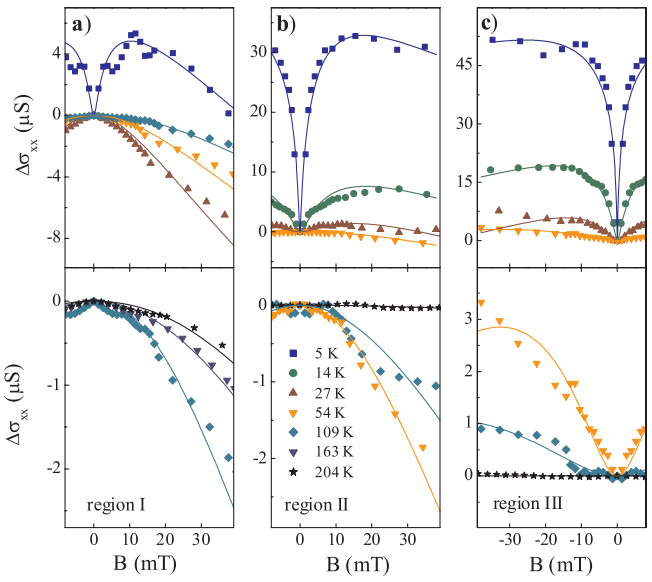

FIG. 3 (color online). (a),(b),(c) Evolution of the magnetoconductance with increasing temperature in the three studied regions, showing a transition from positive to negative low-field magnetoconductance. Bottom panels show the results at high temperatures. Solid curves are fits to Eq. (1).

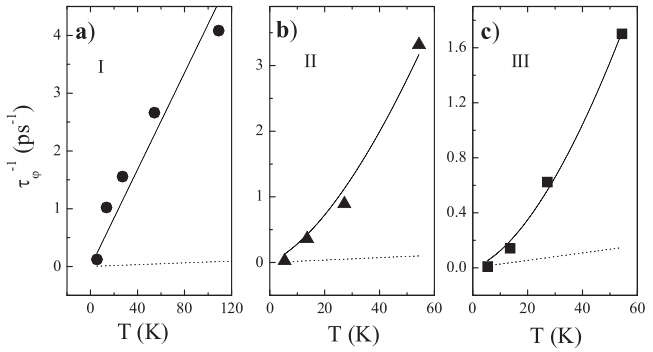

FIG. 4. Temperature dependence of the dephasing rate for the three regions. Solid curves are fits to the electron-electron scattering rates found as a sum of Eq. (3) and (5): (a) $\alpha = 1.5$, $\beta = 0$; (b) $\alpha = 1.5$, $\beta = 2.5$; (c) $\alpha = 0$, $\beta = 2.5$. Dotted lines are electron-phonon rates calculated using Eq. (4).

of the temperature dependence of the classical conductance in [24]. One can see that the electron-phonon rate is too low to explain the experimental values. In addition, the experimental $\tau_\phi^{-1}(T)$ in regions II and III has stronger than linear temperature dependence. The latter excludes not only electron-phonon but also electron-electron scattering in the diffusive regime. The alternative inelastic scattering mechanism, which gives a parabolic temperature dependence, is electron-electron scattering in the ballistic regime, $k_B T\tau_p/\hbar > 1$, when electron interaction is mediated by only a few impurities [25]:

$$\tau_\phi^{-1} = \beta\frac{\pi}{4}\frac{(k_B T)^2}{\hbar E_F}\ln\left(\frac{2E_F}{k_B T}\right). \quad (5)$$

This dependence, with a coefficient β of the order of unity, has been observed in experiments on high-mobility 2D systems at low temperatures [26]. In region I where the transition temperature $k_B T_0\tau_p/\hbar \sim 1$ between the two regimes is high, $T_0 \sim 80$ K, the dephasing rate can be satisfactorily explained by the diffusive electron-electron interaction, Eq. (3). In regions II and III with $T_0 \sim 60$ K and 40 K, respectively, the dephasing rate can be represented as a sum of the two rates, Eq. (3) and (5). Therefore, our results show that it is electron-electron scattering which is the main source of high-temperature dephasing in graphene, due to weak electron-phonon scattering.

In summary, we show that electron antilocalization in graphene, a consequence of the Berry phase π, can be realized experimentally. It can be seen under the conditions when the dephasing time is made small enough compared with the elastic inter- and intravalley scattering times. Our experiments show that quantum interference in graphene can exist at extremely high temperatures due to suppressed electron-phonon scattering.

We are grateful to D. W. Horsell, I. Gornyi, and E. McCann for reading the manuscript and valuable comments, and acknowledge support from the EPSRC grant EP/D031109.

[1] E. McCann, K. Kechedzhi, V. I. Fal'ko, H. Suzuura, T. Ando, and B. L. Altshuler, Phys. Rev. Lett. **97**, 146805 (2006).
[2] A. F. Morpurgo and F. Guinea, Phys. Rev. Lett. **97**, 196804 (2006).
[3] G. Bergman, Phys. Rep. **107**, 1 (1984).
[4] C. W. J. Beenakker and H. Van Houten, *Solid State Physics*, edited by H. Ehrenreich and D. Turnbull (Academic Press Inc., San Diego, 1991) Vol. 44, p. 1.
[5] A. K. Savchenko, A. S. Rylik, and V. N. Lutskii, Zh. Eksp. Teor. Fiz. **85**, 2210 (1983) [Sov. Phys. JETP **58**, 1281 (1983)].
[6] C. Schierholz, T. Matsuyama, U. Merkt, and G. Meier, Phys. Status Solidi B **233**, 436 (2002).
[7] T. Nihei, Y. Suzuki, M. Kohda, and J. Nitta, Phys. Status Solidi C **3**, 4239 (2006).
[8] J. B. Miller, D. M. Zumbühl, C. M. Marcus, Y. B. Lyanda-Geller, D. Goldhaber-Gordon, K. Campman, and A. C. Gossard, Phys. Rev. Lett. **90**, 076807 (2003).
[9] D. Huertas-Hernando, F. Guinea, and Arne Brataas, Phys. Rev. B **74**, 155426 (2006).
[10] X. Wu, X. Li, Z. Song, C. Berger, and W. A. de Heer, Phys. Rev. Lett. **98**, 136801 (2007).
[11] R. V. Gorbachev, F. V. Tikhonenko, A. S. Mayorov, D. W. Horsell, and A. K. Savchenko, Phys. Rev. Lett. **98**, 176805 (2007).
[12] F. V. Tikhonenko, D. W. Horsell, R. V. Gorbachev, and A. K. Savchenko, Phys. Rev. Lett. **100**, 056802 (2008).
[13] D. W. Horsell, F. V. Tikhonenko, R. V. Gorbachev, and A. K. Savchenko, Phil. Trans. R. Soc. A **366**, 245 (2008).
[14] J. Eroms and D. Weiss, New J. Phys. **11**, 095021 (2009); Y.-F. Chen, M.-H. Bae, C. Chialvo, T. Dirks, A. Bezryadin, and N. Mason, arXiv:0906.5090.
[15] S. V. Morozov, K. S. Novoselov, M. I. Katsnelson, F. Schedin, L. A. Ponomarenko, D. Jiang, and A. K. Geim, Phys. Rev. Lett. **97**, 016801 (2006).
[16] K. S. Novoselov, A. K. Geim, S. V. Morozov, D. Jiang, Y. Zhang, S. V. Dubonos, I. V. Grigorieva, and A. A. Firsov, Science **306**, 666 (2004).
[17] K. S. Novoselov, A. K. Geim, S. V. Morozov, D. Jiang, M. I. Katsnelson, I. V. Grigorieva, S. V. Dubonos, and A. A. Firsov, Nature (London) **438**, 197 (2005).
[18] K. Kechedzhi, D. W. Horsell, F. V. Tikhonenko, A. K. Savchenko, R. V. Gorbachev, I. V. Lerner, and V. I. Fal'ko, Phys. Rev. Lett. **102**, 066801 (2009).
[19] M. E. Gershenzon, V. N. Gubankov, and Yu. E. Zhuravlev, JETP Lett. **35**, 576 (1982).
[20] T. Stauber, N. M. R. Peres, and F. Guinea, Phys. Rev. B **76**, 205423 (2007).
[21] E. H. Hwang and S. Das Sarma, Phys. Rev. B **77**, 115449 (2008).
[22] B. L. Altshuler, A. G. Aronov, and D. E. Khmelnitsky, J. Phys. C **15**, 7367 (1982).
[23] B. L. Altshuler, A. G. Aronov, A. I. Larkin, and D. E. Khmelnitsky, Zh. Eksp. Teor. Fiz. **81**, 768 (1981) [Sov. Phys. JETP **54**, 411 (1981)].
[24] J. H. Chen, C. Jang, S. Xiao, M. Ishigami, and M. S. Fuhrer, Nature Nanotech. **3**, 206 (2008).
[25] B. N. Narozhny, G. Zala, and I. L. Aleiner, Phys. Rev. B **65**, 180202 (2002).
[26] R. Taboryski and P. E. Lindelof, Semicond. Sci. Technol. **5**, 933 (1990); Y. Y. Proskuryakov, A. K. Savchenko, S. S. Safonov, M. Pepper, M. Y. Simmons, and D. A. Ritchie, Phys. Rev. Lett. **86**, 4895 (2001); A. S. Price, A. K. Savchenko, B. N. Narozhny, G. Allison, and D. A. Ritchie, Science **316**, 99 (2007).